Soft Matter

PAPER

View Article Online
View Journal | View Issue

Cite this: *Soft Matter*, 2018, **14**, 5256

Controlled self-assembly of stomatosomes by use of single-component fluorinated dendritic amphiphiles†

H. v. Berlepsch,[ab] B. N. S. Thota,[c] M. Wyszogrodzka,[c] S. de Carlo,[d] R. Haag*[c] and C. Böttcher*[a]

A series of novel non-ionic amphiphiles with dendritic oligoglycerol head groups of different generations ([G1]–[G3]) and lipophilic/fluorophilic tail segments, comprising single or double tail alkyl chains, C_8F_{17}-perfluoro rod segments as well as flexible spacer groups of different lengths were designed and synthesized. We expected that the differences in the size of the dendritic head groups in combination with perfluorinated segments would have an impact on the supramolecular structures formed in aqueous solution if compared with the hydrogenated analogues. Investigating the self-assembly behavior mainly by cryogenic transmission electron microscopy (cryo-TEM) and cryo-electron tomography (cryo-ET) we found as a new result the formation of perforated bilayer vesicles (stomatosomes) and bicontinuous network structures. Surprisingly, we have observed stomatosome formation by self-assembly of single component fluorinated dendritic amphiphiles. These assembly structures turned out to be extremely robust against harsh conditions, although there are strong indications that they represent non-equilibrium structures, which eventually transform into a bicontinuous cubic network structure of double diamond symmetry. In general, the molecular asymmetry of amphiphiles tuned by chemical design induced the expected trend from spherical micelles through worm-like micelles to perforated bilayers and three-dimensional network structures.

Received 2nd February 2018,
Accepted 1st March 2018

DOI: 10.1039/c8sm00243f

rsc.li/soft-matter-journal

Introduction

There is currently a growing interest in studying the self-assembly of dendritic amphiphiles due to their unusual packing behavior in supramolecular assemblies and the potential engineering of defined nanostructures through a rational molecular design.[1] For potential applications in nanomedicine and nanobiotechnology non-ionic systems are of particular interest as their pH independence makes them useful *e.g.* in view of the efficient drug delivery of hydrophobic agents.[2]

In previous studies we could demonstrate that amphiphiles with dendritic oligoglycerol head groups, including chiral derivatives, are promising for the construction of structurally defined supramolecular assemblies with low polydispersity.[3–6] This type of molecule with extended multifunctional head groups lies at the boundary of classical surfactants and amphiphilic polymers. Their multifunctionality makes them advantageous over classical amphiphiles with linear head groups (*e.g.* comprised of ethoxylate units) as they were proven to produce structurally persistent nanostructures.[3,7–9]

The dendritic amphiphiles studied so far[3–6] combined non-ionic dendritic oligoglycerol head groups of different generations ([G1]–[G3]) with long alkyl chains as lipophilic tail segments, comprising aromatic or non-aromatic linker groups. On the other hand we knew from previous investigations of amphiphilic block copolymers[10] that amphiphiles with fluorinated segments tend to aggregate in aqueous solution into structures of lower curvature as compared to their hydrocarbon analogues. Another effect of fluorination is the tendency for microphase separation within the hydrophobic area of certain aggregates (multicompartment micelles of block copolymers) due to the poor compatibility of the hydro- and fluorocarbon segments.[11] A positive side effect is that due to the high electron density of fluorine supramolecular structures incorporating fluorine moieties can be imaged with improved contrast by cryo-transmission electron microscopy compared

[a] *Forschungszentrum für Elektronenmikroskopie, Institut für Chemie und Biochemie, Freie Universität Berlin, Fabeckstraße 36a, 14195 Berlin, Germany. E-mail: christoph.boettcher@fzem.fu-berlin.de*
[b] *Core Facility BioSupraMol, Institut für Chemie und Biochemie, Freie Universität Berlin, Fabeckstraße 36a, 14195 Berlin, Germany*
[c] *Institut für Chemie und Biochemie, Organische Chemie, Freie Universität Berlin, Takustraße 3, 14195 Berlin, Germany. E-mail: haag@chemie.fu-berlin.de*
[d] *Thermo Fisher Scientific, Achtseweg Noord 5, 5651 GG Eindhoven, The Netherlands*

† Electronic supplementary information (ESI) available. See DOI: 10.1039/c8sm00243f

to its hydrogenated analogue.[11] Taken all together this has set the starting point to study novel variants of dendritic amphiphiles combined with perfluorinated segments and to follow up the question, whether these molecules follow the general trend of assembly behavior of their hydrogenated analogues in terms of their molecular asymmetry, or in other words the well-known concept of packing parameter.[12] Moreover, we were interested to see if novel supramolecular assembly structures can be generated by exploiting the specific structure inducing effects of dendritic head groups and perfluorinated segments. Therefore, we targeted the synthesis design regarding the selective variation of head group size, chain length and number as well as spacer length (Fig. 1). We investigated the assembly behavior and structure mainly based on cryogenic transmission electron microscopy (cryo-TEM) data including cryo-electron tomography (cryo-ET) measurements.

Polyglycerol dendrimers that contain a perfluorinated shell have previously been synthesized[13] and analyzed with respect to their aggregation behavior.[14] These dendritic polymers have been employed as a supramolecular, homogeneous support for a perfluoro-tagged Pd catalyst in Suzuki coupling.[13] Also the influence of perfluoroalkyl tails in the self-assembly of classical surfactants is well documented in the literature.[15–17] It is so far not clear, however, how perfluoroalkyl tails affect the self-assembly of the amphiphiles with dendritic oligoglycerol head groups in water.

The reasons for the specific behavior of fluorinated segments are the pronounced hydrophobicity (fluorophilicity) and the stiffness of the fluorocarbon chains as well as their larger cross-sectional area, which results in a different molecular packing parameter as compared to the hydrocarbon analogues.[18] Thus, cylindrical micelles or planar structures instead of spherical micelles have frequently been reported.[19,20] Besides cylindrical micelles and planar bilayer structures more complex morphologies such as branched cylindrical micelles, rings, perforated bilayer vesicles, and mesh phases have been reported.[21–27] In particular, the morphologies with non-constant interfacial curvatures (bicontinuous phases) are interesting at a fundamental level in order to understand why they form.[28,29]

Fluorinated amphiphiles are also interesting for applications. For example, fluorinated vesicles are expected to possess a high drug encapsulation stability. For that reason, a great diversity of fluorinated amphiphilic systems has been synthesized and analysed with respect to the aggregation behavior.[15–17,30] Among them are single and double-chain fluorinated compounds, amphiphiles with mixed chains, one fluorinated, the other hydrogenated, or mixtures of hydrogenated and fluorinated amphiphiles.[17] However, most of these amphiphiles comprised ionic head groups.

Results

Stirring at ambient temperature was sufficient to solubilize most of the compounds in water giving clear or slightly turbid solutions within a concentration range of 0.5 and 1% (w/v), suitable for a complementary DLS and cryo-TEM analysis. Only double-chained compounds with dendritic head groups of the first generation ([G1]) were insoluble in water and were thus excluded from this study. Alternative methods for the solubilization of the compounds in water such as ultrasonication or heat treatment were also used. Short sonication times (1–2 minutes) or heat treatments (1–2 hours at 60–70 °C) had generally no strong effect on the micellar morphology, whereas harsher treatments (ultrasonication for up to 45–60 minutes and further annealing above the chain melting temperature) affected the morphology of the assemblies as will be discussed below.

Single-tailed amphiphiles [Gn]-C_x-R_f

Generation 1 derivatives. The critical micelle concentration of [G1] molecules (**1** ([G1]-C_3-R_f), **2** ([G1]-C_6-R_f)) with single chains was determined by surface tension measurements (Fig. 2). The cmc values are in the concentration range of 10^{-5} M for the two compounds, *i.e.* a clear dependency on the chemical structure cannot be inferred from the obtained data within the limits of error. A pronounced amphiphilicity of these molecules can be noticed by the lowering of the surface tension values above the cmc.

The cryo-TEM studies of amphiphiles **1** ([G1]-C_3-R_f) and **2** ([G1]-C_6-R_f) (Fig. 3) revealed the formation of worm-like assemblies for **1** and of perforated bilayer vesicles as well as planar patches of network structures for **2**. Following the contour of the individual worm-like assemblies formed by amphiphile **1** ([G1]-C_3-R_f) (Fig. 3a and b) varying diameters and contrast can be noted. Sections in face-on orientation give a well-defined width of about 7 nm, whereas sections orientated in side-view orientation reveal a thickness of about 2.6 nm. A similar morphology was recently reported for another fluorinated surfactant.[21] In both cases narrow ribbons are formed instead of the common cylindrical micelles.

The anisometric cross-section is a typical effect of the fluorinated chain segments. While the chains prefer a packing towards bilayers, the bulky head groups favor a cylindrical curvature. The formation of narrow ribbons seems to be a compromise.

The representative cryo-TEM micrograph of a solution of amphiphile **2** ([G1]-C_6-R_f) with a longer alkyl spacer reproduced in Fig. 3c reveals vesicles and network structures. The vesicles can be discriminated by a high-contrast rim and their overall shape deviates from a perfect spherical geometry normally found with lipid vesicles. However, the biggest difference with respect to the lipid vesicle is the porous membrane, which seems to consist of a loose irregular network of branched cylindrical fibres. The mean diameter of the vesicles is about 200 nm in agreement with the corresponding DLS data. The mesh-size in networks is about 20 nm. The DLS data for both compounds are shown in Fig. 3d.

Another type of vesicle with more or less regularly arranged perforations is found for the double-chained [G2] amphiphiles, which will be discussed in detail below. Such perforated bilayer vesicles have been systematically examined earlier by M. Almgren and coworkers,[26] who also coined the term ''stomatosome'' for

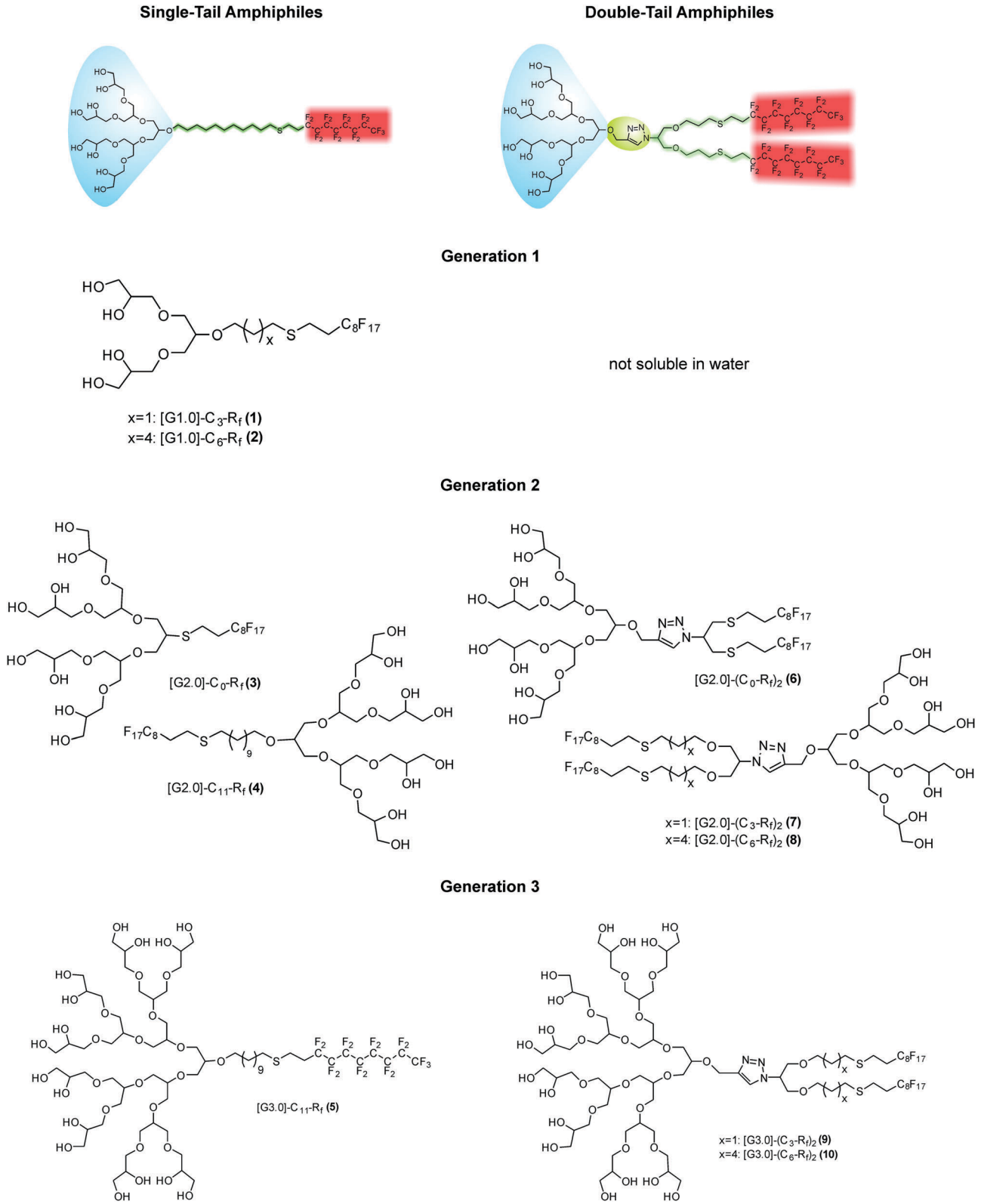

Fig. 1 Schematic structural design of the new perfluoroalkyl non-ionic glycerol based amphiphiles.

this fascinating structure. So far stomatosomes have only been identified in multicomponent surfactant[31–34] and block copolymer systems[34,35] in narrow temperature and concentration regimes often coexisting with other structures. Before we provide detailed results, some key aspects of the electron microscopic characterization of stomatosomes have to be given first.

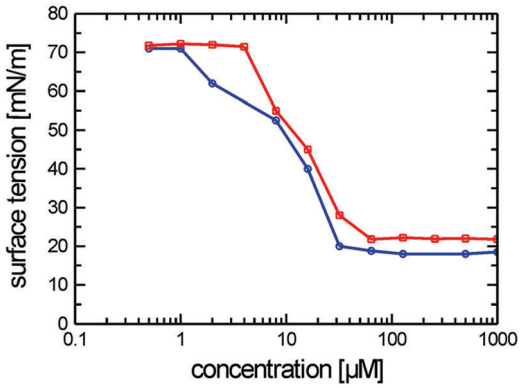

Fig. 2 Surface tension measurements of [G1] amphiphiles **1** ([G1]-C_3-R_f) (red line) and **2** ([G1]-C_6-R_f) (blue line).

Computer model data of a stomatosome structure, which can be perceived as a perforated vesicle, together with two sections through a reconstructed 3D volume of experimental data obtained from cryo-electron tomographic (cryo-ET) reconstruction data (amphiphile **8** ([G2]-(C_6-R_f)$_2$)) are shown in Fig. 4. For didactic reasons we anticipate the data for a double-chained compound, as it shows nearly perfect stomatosomes.

It is noteworthy that a stomatosome presents a dotted outer rim in projection images (see Fig. 4b), which is indicative of the spherical geometry (high contrast) and perforations (dots) in the membrane. Due to its perpendicular orientation to the electron beam the rim appears darker than the rest of membrane. The size and pattern of the perforations differ from the surface view and reflect the superposition of densities from the top and bottom layers. This finding renders the measurements of mesh size, mesh width or mesh morphology (projection images misleadingly suggest an ellipsoidal cross-section of the meshes) from individual projection images (as obtained from individual TEM images) difficult and requires information of the individual layer pattern in three dimensions. By performing the cryo-electron tomography of a real representative stomatosome preparation of compound **8** ([G2]-(C_6-R_f)$_2$), it can be seen (Fig. 4c and d) that the membrane consists of a regular mesh with a nearly circular cross-section of the branch points with a diameter of 5.5 nm. The interior volume of the vesicle is hollow and filled with water. The perforations are arranged in a hexagonal pattern with a center-to-center distance of 18.2 nm and an individual diameter of 6.2 nm.

Generation 2 and 3 derivatives. To study how the geometry of the dendritic head group affects the aggregation behavior of the single-chained compounds we investigated [G2] and [G3] homologues (Fig. 1). All the aggregates were characterized by DLS and cryo-TEM. The DLS data predicted small micelles with mean hydrodynamic diameters of about 6.2 nm for compounds **3** ([G2]-C_0-R_f) and of about 9 and 8 nm for compounds **4** ([G2]-C_{11}-R_f) and **5** ([G3]-C_{11}-R_f), respectively. The narrow size distribution in all cases point to the formation of monodisperse spherical micelles. These results were well confirmed by the respective cryo-TEM data (Fig. 5). The completely expanded length of molecule **4** ([G2]-C_0-R_f) is about 4.5 nm and determines the maximum micelle radius. The bulky head groups

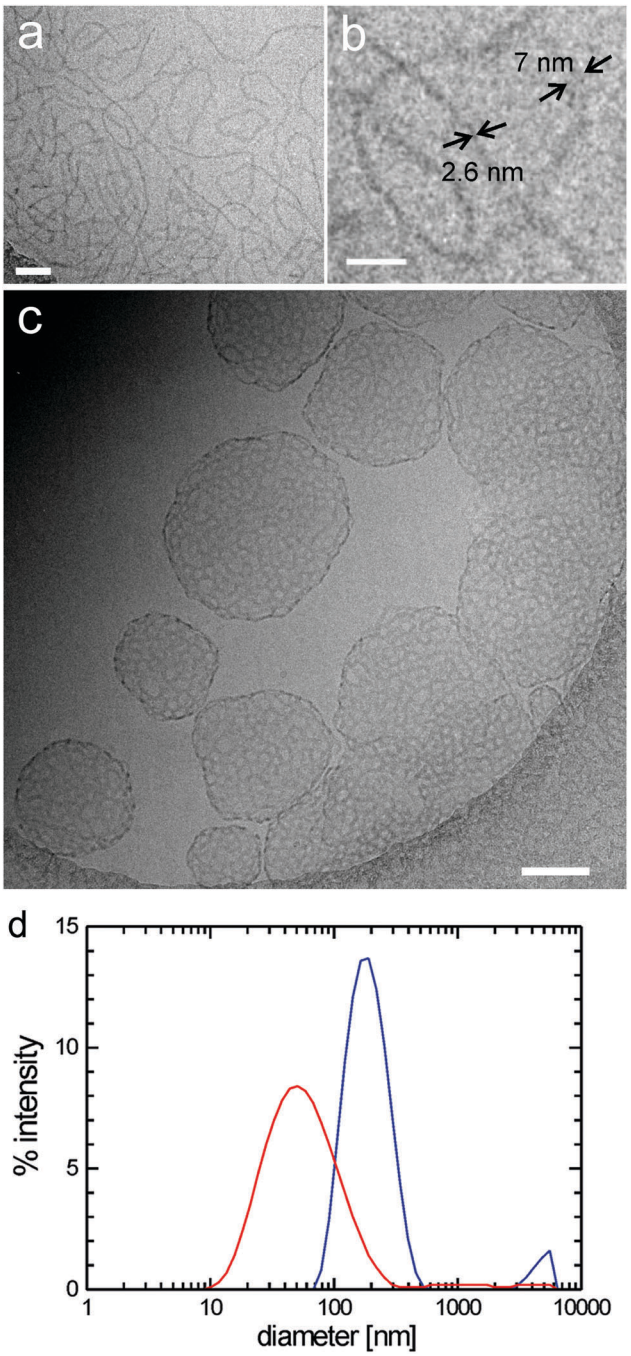

Fig. 3 (a and b) Cryo-TEM images of compound **1** ([G1]-C_3-R_f) reveal ribbon-like structures. Scale bars are 50 nm (a) and 20 nm (b). (c) Cryo-TEM images of compound **2** ([G1]-C_6-R_f) show vesicle-like structures with high contrasts rims, which consist of irregularly arranged branched micellar fibers. Scale bar is 100 nm. Amphiphile concentrations: 1% (w/v). (d) Size distributions obtained by DLS from dilute aqueous solutions of amphiphiles **1** (red line) and **2** (blue line). While the distribution function for the entangled network of worm-like micelles (amphiphile **1**) allows no straightforward interpretation in terms of aggregate size determination, a mean hydrodynamic diameter of ~200 nm is obtained for the perforated vesicles formed by amphiphile **2** in agreement with the cryo-TEM data. Amphiphile concentrations: 0.1% (w/v).

induce a strong asymmetry of the molecules, which even for a larger hydrophobic spacer (compounds **4** ([G2]-C_{11}-R_f) and

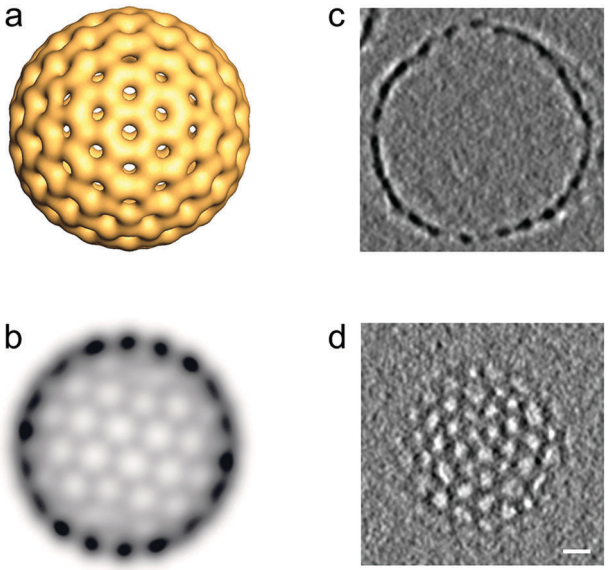

Fig. 4 (a) 3D-Model illustrating the structural organization of a regular stomatosome and (b) corresponding projection image simulating the appearance in a TEM image (more details in Fig. 8). Note that the pattern of the perforations on the surface (number and size) and the projection pattern differ due to the superposition effects in the latter. (c) Transections through the central volume and (d) the outer membrane of a 3D-reconstructed stomatosome obtained by cryo-ET of compound **8** ([G2]-(C_6-R_f)$_2$). The regular perforated pattern of the outer membrane and the hollow inner volume is unambiguously proven. Scale bar in panel (d) is 10 nm.

5 ([G3]-C_{11}-R_f)) enforces the formation of solely spherical micelles. Particularly striking is the homogeneous particle density (Fig. 5e), *i.e.* the hydrophobic core is indistinguishable from the outer head group shell, which is different from micelle preparations of amphiphiles with alkyl chains, where we observe significantly less density for the hydrophobic core (Fig. 5d). The effect is obviously related to the perfluorinated chain segments due to their higher scattering contrast compared to alkyl chains.[11]

Double-tailed amphiphiles [Gn]-(C_x-R_f)$_2$

Due to their predominant hydrophobic character double-chained amphiphiles with [G1] heads are insoluble in water. Therefore, we have focused on the reasonably water soluble [G2] and [G3] homologues. By analogy to the single-tailed amphiphiles the length of the hydrocarbon spacer was additionally varied. To prepare solutions at a standard concentration of 0.5 wt%, suitable for DLS as well as for cryo-TEM measurements, different methods for the solubilization of [G2] compounds were employed in order to study their impact on the assembly structures, namely short time ultrasonication (1–2 minutes), heat treatment (up to 70 °C) or simple stirring in water. No morphological differences could be detected dependent on the method used. Likewise, a tenfold dilution of aggregated solutions had no effect on the aggregate morphology. We will show below, however, that harsher conditions affect the aggregate morphology.

Generation 2 derivatives. The aggregation behavior of [G2] amphiphiles (**6–8**) ([G2]-(C_0-R_f)$_2$, [G2]-(C_3-R_f)$_2$, [G2]-(C_6-R_f)$_2$) differing mainly in the spacer length was initially studied by surface tension and DLS measurements. Even at the highest concentration (0.5 wt%) no considerable decrease in the surface tension was observed, indicating slow dynamics. The size distributions of aggregates obtained by DLS are depicted in Fig. 6. The broadened curves point to a certain degree of polydispersity at mean hydrodynamic diameters ranging between 70 and 300 nm.

Cryo-TEM revealed the stomatosomes to be the dominant morphology for all samples irrespective of the hydrocarbon spacer length, C_x. A typical micrograph showing several stomatosomes of ~200 nm diameter is presented in Fig. 7a (see also Fig. 4c and d) for compound **8** ([G2]-(C_6-R_f)$_2$). Besides stomatosomes with high contrast outer rim mesh-like objects of low and uniform contrast are identified for all the compounds. A typical example of the latter type of structures for compound **7** ([G2]-(C_3-R_f)$_2$) can be seen in the top area of Fig. 7b. The Fourier transformation of this object shows a clear hexagonal pattern of spots confirming its highly ordered architecture, comparable to the pattern of the stomatosomal membrane shown in Fig. 4d.

Comparable to conventional lipid vesicle structures,[36] different structural motifs of the stomatosomal organization are observed. This heterogeneity in size and shape depends on the particular sample preparation method and is reflected in the DLS data. Thus, in addition to single-layered stomatosomes, concentrically and non-concentrically multi-layered stomatosomes are found. Non-concentrically multi-layered stomatosomes can be unambiguously identified only by cryo-ET, because this technique provides three-dimensional images of the samples that are free of the inherent overlapping effects of projection images. This question has not been adequately addressed, however, in the present studies. Most likely, we are dealing with real multi-layered stomatosome in those cases, where a smaller stomatosome appears to be trapped inside a larger one (in the projection image), while their walls don't cross, but only touch each other (*cf.* the transmission image shown in Fig. 7c).

Moreover, planar mesh-like assemblies can be detected, which will be discussed below. A typical cryo-TEM micrograph of compound **7** ([G2]-(C_3-R_f)$_2$) is depicted in Fig. 7c. A particularly well-ordered example of a concentrically multi-layered stomatosome is shown in Fig. 7d for compound **6** ([G2]-(C_0-R_f)$_2$). The four-fold membrane layer and the regular perforations are well distinguishable. In some areas the stacked layers are precisely aligned, which creates a particularly well-defined hexagonal pattern of high contrast. Besides the multiple stacking of the membrane (four layers) the outer boundary reveals the typical regular spot-like pattern expected from stomatosomes in projection view (compare Fig. 4).

In the tightly packed multi-layered stomatosomes (Fig. 7d) the layer repeat spacing, D, is about 7 nm, whereas the individual membrane layer thickness, D_L, is about 5 nm. Given a typical water layer of about 2 nm these distances are comparable with those of classical multi-walled vesicles composed of smooth membranes.[37] In order to look for a possible dependence of characteristic distances on the length of the hydrocarbon spacer, we measured the membrane thickness in

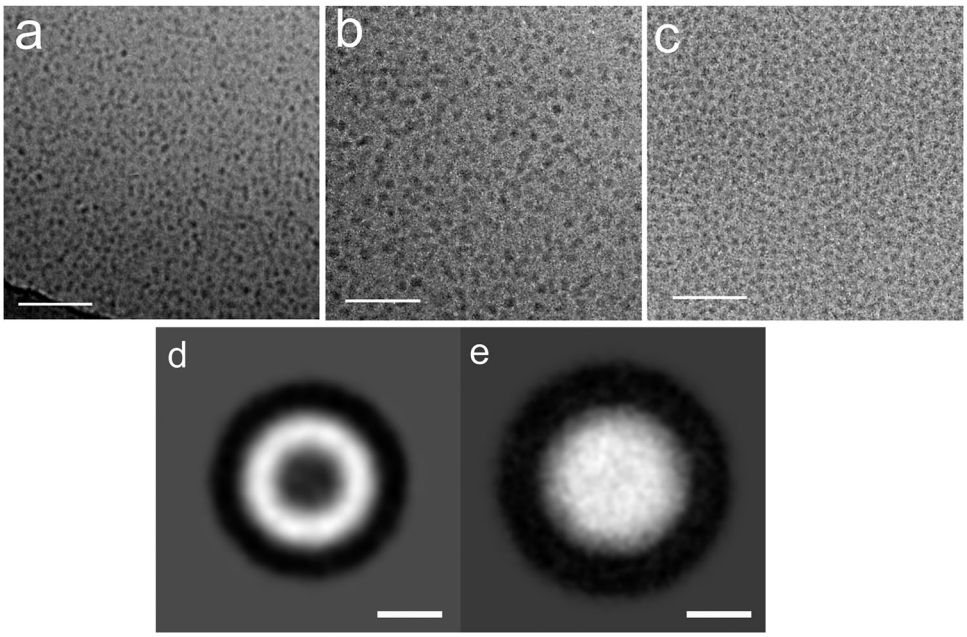

Fig. 5 Cryo-TEM images of the compounds **3** ([G2]-C_0-R_f) (a), **4** ([G2]-C_{11}-R_f) (b) and **5** ([G3]-C_{11}-R_f) (c) show spherical micelles of 4 nm (**3**) and 7 nm (**4**, **5**), respectively. Amphiphile concentrations: 1% (w/v). (d) Summing of ~100 centered individual images of micelles (diameter is ~5 nm) formed by an [G2] amphiphile with an C_{11} alkyl chain and a monoaromatic spacer reveals density differences between the corona (high density = white) and core (low density = dark). (e) Summing of 100 centered micelles of compound **4** (with fluorinated hydrophobic tail) shows a homogeneous white particle (diameter is ~7 nm) due to a similar electron density in corona and core volume. Note that the contrast in (d) and (e) is inverted (micelles are dark in the original cryo-electron micrographs) due to image processing convenience. Scale bars are 50 nm (a–c) and 3 nm (d and e).

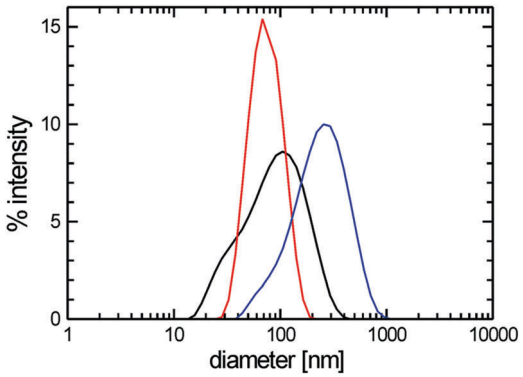

Fig. 6 Diameter distributions obtained by DLS from diluted aqueous solutions of amphiphiles **6** ([G2]-$(C_0$-$R_f)_2$) (blue line), **7** ([G2]-$(C_3$-$R_f)_2$) (red line), and **8** ([G2]-$(C_6$-$R_f)_2$) (black line). Amphiphile concentrations: 0.1% (w/v).

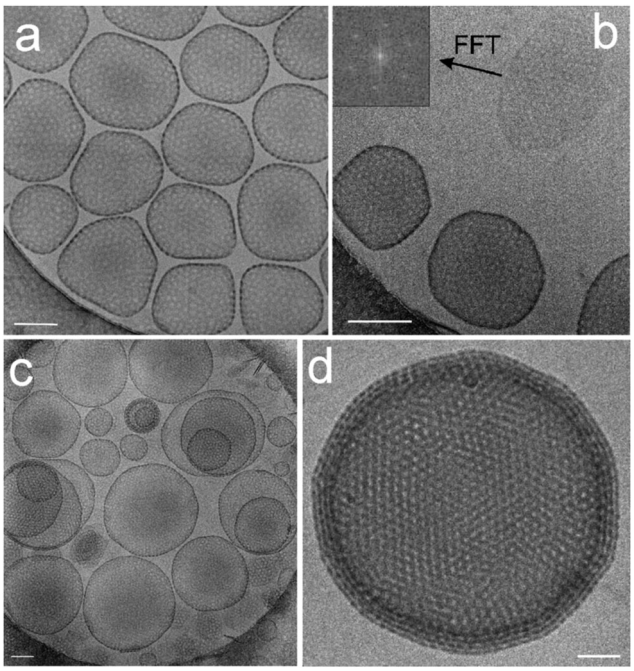

Fig. 7 (a) Cryo-TEM images of the compound **8** ([G2]-$(C_6$-$R_f)_2$) showing single-layered stomatosomes. 3D data from this preparation are shown above in Fig. 4c and d. Scale bar is 100 nm. (b) Stomatosomes and the perforated layer with a regular hexagonal pattern of holes as indicated by the corresponding FFT (inset) of compound **6** ([G2]-$(C_0$-$R_f)_2$) without spacer. Scale bar is 100 nm. (c) Single-layered, concentrically and non-concentrically multi-layered stomatosomes of compound **7** ([G2]-$(C_3$-$R_f)_2$). Scale bar is 100 nm. (d) Four-fold stacked multi-layered stomatosome of compound **6**. Scale bar is 50 nm. Concentration of solutions: 1% (w/v).

stacked arrangements of all three compounds and obtained the dependencies plotted in Fig. 8C.

The membrane layer thickness, D_L, increases with the molecular spacer length, x. The estimated values roughly agree with twice the fully extended molecular lengths of the molecule, supporting the bilayer model for the constituent membranes. The repeat spacing of concentrically multi-layered lamellae, D, shows the same trend. Thus, the width of the interfacial water layer: $D - D_L = D_W \approx 2$ nm is constant. The mesh size (hexagonal lattice constant), a, determined by Fourier Transform with high accuracy, increases clearly with the spacer length. The determination of the hole size, D_H, is, however, error-prone due to

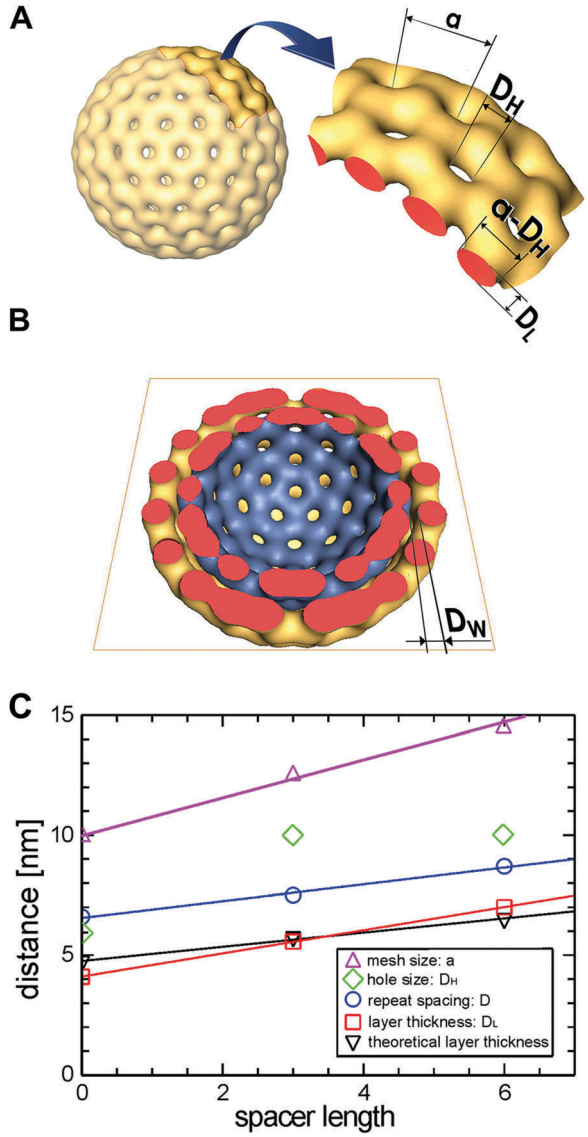

Fig. 8 (A) Model of a stomatosome with designation of its geometrical parameters: membrane layer thickness: D_L, mesh size: a, hole size: D_H, mesh width ($a - D_H$). (B) Model from (A) with top half removed and interfacial water layer thickness designated as D_W. (C) Effect of the spacer length, x, of compounds [G2]-$(C_x\text{-}R_f)_2$ (**6–8**) on the structural characteristics of stomatosomes derived from cryo-TEM data.

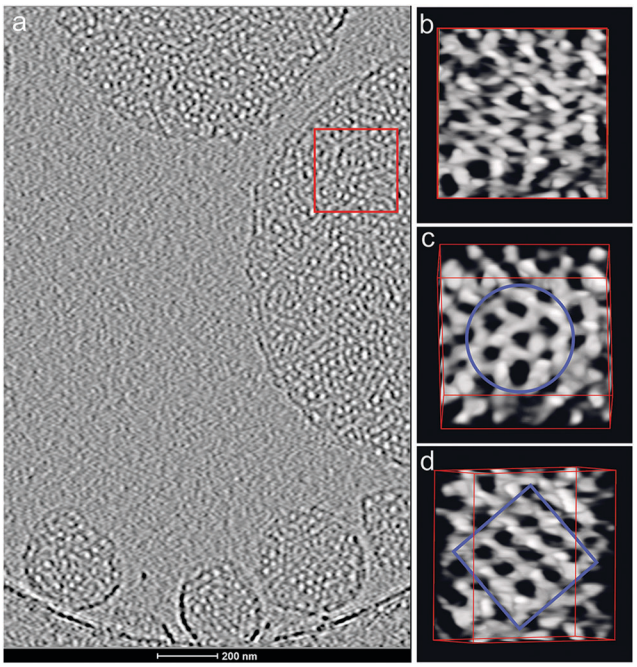

Fig. 9 (a) Projection image of a central section of a 3D volume reconstructed from a cryo-tomographic tilt series (±70° tilt range in 2° steps) of compound **7** ([G2]-$(C_3\text{-}R_f)_2$). (b–d) Reconstructed 3D volume segment in voltex representation (AMIRA software)[41] from the boxed area of the mesh in three orientations reveals a bicontinuous cubic phase: (b) top view of the reconstruction boxed from the area marked left. (c) In the [111] view orientation a hexagonal mesh pattern becomes visible. (d) Reconstructed volume oriented in [100] orientation reveals a cubic mesh pattern. The tilt angle orientation with respect to the encircled area in (c) is indicated and amounts to 45°.

the superposition effects in projection views and a clear trend with respect to x cannot be derived (see also Fig. 4). From the tomographic reconstruction presented in Fig. 4 we can however conclude that the cross section of the mesh grids, or the mesh width ($a - D_H$), is circular and agrees roughly with the layer thickness, D_L.

As mentioned above, conventional cryo-TEM imaging results in 2D projection images of a three-dimensional object and hence the interpretation of images is particularly problematic in terms of the assemblies' spatial organization. The missing three-dimensional information can in principle be retrieved by a tomographic technique where an image series is recorded at systematically varied tilt-angles.[38–40] It was of particular interest to reveal the interior structure of the perforated layers and concomitantly confirm the structural organization of the stomatosomes. For compound **8** ([G2]-$(C_6\text{-}R_f)_2$) we had shown sections of a tomographic reconstruction of a stomatosome in Fig. 4, which proved its hollow morphology. Moreover, most of the perforated mesh patches also present in the preparation (Fig. 7b), turned out to be planar perforated sheets with a thickness of the order of the molecular bilayer. In some cases, however, the tomographic data revealed a surprisingly more complex structure of such meshes although the individual projection images gave no indication for significant differences (Fig. 9).

The right column in Fig. 9(b–d) shows different orientations of a reconstructed three-dimensional subvolume (voltex representation in AMIRA software[41]) taken from the indicated area (Fig. 9a) of a mesh, which reveals a particularly well-defined three-dimensional order and a dimension in the z-direction exceeding the dimension of an individual flat bilayered membrane as shown in Fig. 7b by a factor of 4 (≈30 nm).

Though the morphology in top view orientation (Fig. 9b) appears irregular, tilted views, however, reveal a hexagonal and a corresponding cubic pattern upon further tilting of 45° (Fig. 10). A skeletal representation of the three-dimensional branching pattern, additionally included in the figure, facilitates the understanding of the overall organization. The structural unit is a

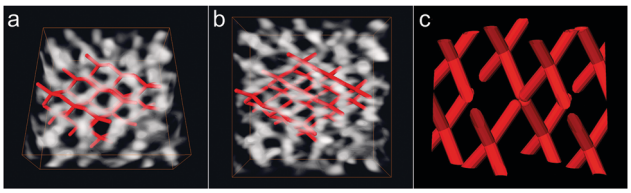

Fig. 10 (a and b) Reconstructed volume as shown in Fig. 9(b–d) at different view angles (~35° around a horizontal tilt axis) together with a skeletal model (red) highlighting the connectivity of the pattern in its three-dimensional organization. (c) Detail of the skeletal model accentuating the tetrapod connectivity of the motif.

tetrapod, where each branching point connects four neighbors. The opening angle slightly deviates from a tetrahedral geometry (109.5° *vs.* 105.9°) if it were an ideal diamond structure. However, tilting the reconstructed volume from the hexagonal orientation by about 45° reveals a nearly cubic pattern, which indicates the structural similarity to a double diamond geometry. Ordered bicontinuous cubic phases are frequently observed in complex fluids.[42] However, these ordered networks are mostly characterized by three-fold coordinated network lattices (gyroid phases). The present tetrapod organization is rare and has so far only been identified for lipid–water systems,[43] surfactants[44] and quite recently for a thermotropic liquid crystalline bolaamphiphile.[45] In the case of diblock copolymers the double gyroid structure is energetically favored in general, but for certain stereoregular and graft block copolymers a thermodynamically stable double diamond has also been detected recently.[46,47]

One has to emphasize that the three-dimensional organization of the reconstructed bicontinuous structure shows frequent defects. Although the above ordered organization is clearly visible in this particular volume, most areas lack or show only incomplete branching connections. This finding might strengthen the conclusion that this kind of structure represents a transitional non-equilibrium structure (see below).

Interestingly, upon closer inspection of the more spherical assemblies in Fig. 9a stomatosome-like assemblies with partially high-contrast outer membrane and a similar three-dimensional branching as found for the bicontinuous meshes can be revealed in the interior volume of these vesicles. Also, here the 3D network is far from being perfectly structured but it is obvious that also this stomatosome-like structure is different from that presented in Fig. 4, where a network-like structuring is exclusively restricted to the outer membrane and the interior volume is hollow. These observations shed new light on the dynamics of these supramolecular assemblies, which obviously indicate the coexistence of intermediate structures. This points clearly to a non-equilibrium nature of stomatosomes and requires an in-depth discussion (see below).

Stability of stomatosomes under harsh preparation conditions

In this section we will have a closer look on the effects of harsher sample preparation methods in terms of their impact on non-equilibrium structures. Under standard conditions with short ultrasonication (1–2 minutes) and heating times (1–2 hours at 70 °C) the aggregate structures turned out to be reproducible and highly robust as demonstrated above. Nevertheless, changes in the morphology induced by extensive sonication (several hours) and by annealing at 70 °C could be proven in some cases.

Effects of ultrasonication. Studies comparing the morphologies of solutions prepared with or without sonication exemplified by compound **8** ([G2]-(C_6-R_f)$_2$) gave a clear effect. Fragments of stomatosomes or perforated layers (those fragments appear in edge-on orientation as contrast rich rods) were observed, when sonication was applied for 2 hours at 45 °C (Fig. 11). Shorter 45 to 60 minutes treatments showed no effect at all. This result indicates the robustness of the assembly structures. We will see below that significant changes in the molecular organization can only be induced by annealing above the melting temperature of the fluorinated chains. Ultrasonication below the melting temperature causes only mechanical disruption of structures.

Temperature effects. Temperature is another experimental parameter, which was thought to have an impact on the supramolecular aggregation process. Because the perfluorinated carbon chains are robust and inflexible the amphiphiles have a high melting temperature.[18] In order to detect the increase of chain motion with temperature we measured the ^{19}F-NMR spectra. As the line width and intensity of the ^{19}F resonance at −83.7 ppm respond sensitively to the gel to liquid-crystalline phase transition temperature, the induced changes can be used to estimate the phase transition temperature.[48] A set of NMR spectra obtained for amphiphile **8** ([G2]-(C_6-R_f)$_2$) is shown in Fig. 12, revealing that chain melting occurred over a broad temperature range between 50 and 70 °C (*cf.* peak intensity *vs.* temperature plot in Fig. S1 in the ESI†). A similar behavior has been observed, virtually independent of the length of hydrocarbon spacer C_x, for the amphiphiles **6** ([G2]-(C_0-R_f)$_2$) and **7** ([G2]-(C_3-R_f)$_2$).

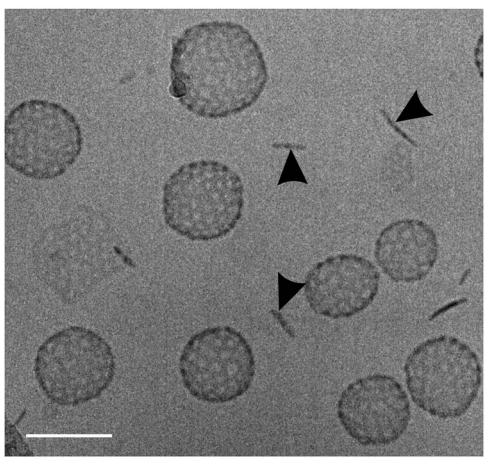

Fig. 11 Cryo-TEM image of compound **8** ([G2]-(C_6-R_f)$_2$) after two hours of ultrasonication at 45 °C. Besides intact stomatosomes bilayered membrane fragments frequently occur, which appear as high contrast rods in edge-on orientation (arrow heads). Scale bar is 100 nm. Amphiphile concentration: 1% (w/v).

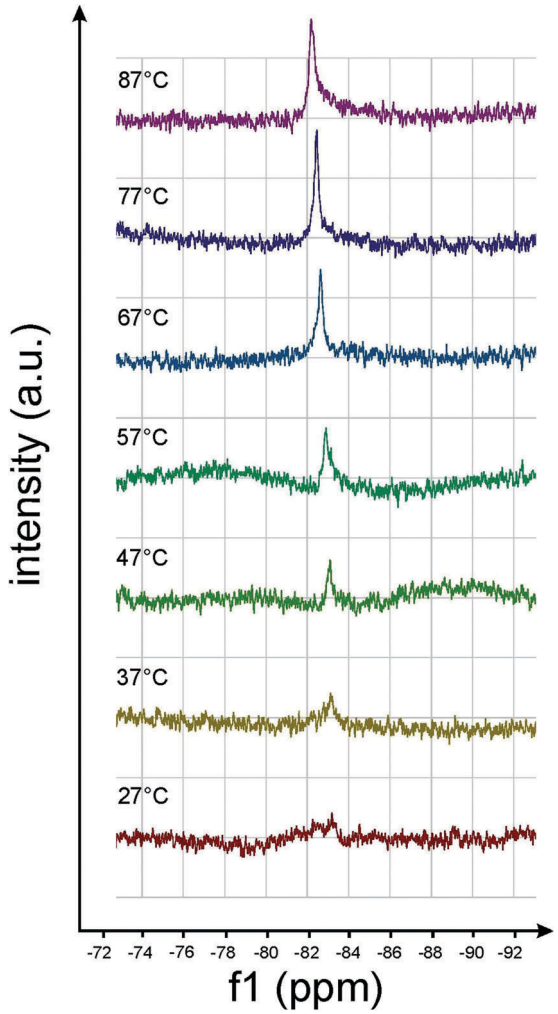

Fig. 12 ^{19}F-NMR spectra of amphiphile **8** ([G2]-(C_6-R_f)$_2$) taken at different temperatures. The intensity increase of the ^{19}F resonance at −83.7 ppm indicates chain melting above ∼50 °C.

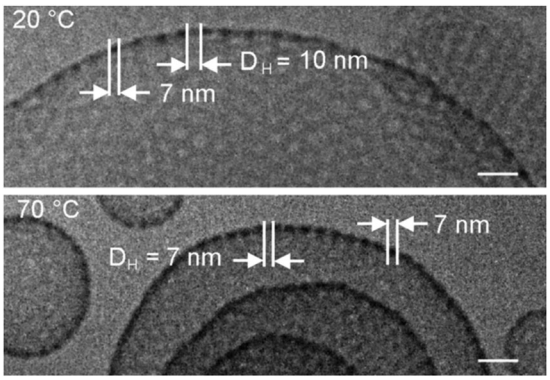

Fig. 13 Cryo-TEM images of compound **7** ([G2]-(C_3-R_f)$_2$) prepared at 20 °C (top) and at 70 °C (bottom), respectively, reveal changes in the diameter of the perforations. The effect can be explained by an increase of the spontaneous curvature by melting of the fluorocarbon chains. Concentration of solutions: 1% (w/v). Scale bar is 25 nm. Respective overview images are presented in the ESI.†

Chain melting significantly affects the size of perforations. Fig. 13 displays micrographs of compound **7** ([G2]-(C_3-R_f)$_2$) vitrified at 20 °C and at 70 °C, respectively (overview images are shown in Fig. S2 and S3 in the ESI†). The stomatosomes show a smaller mesh size when prepared at ∼70 °C. The mesh size, a, decreased in parallel with the hole size, D_H, from about 17 to 14 nm and 10 to 7 nm, respectively, which means that the width of the meshes, ($a - D_H$), remains almost constant (∼7 nm). Changes in the structural organization upon increase of the temperature are known for lipids. Lipid vesicles adopting a crystalline state show a facetted ultrastructure, which disappears in the liquid-crystalline state above the gel-to-liquid-crystalline phase-transition temperature.[49] In the case of classical lipid vesicles the bilayer membrane becomes more flexible and their thickness (D_L) decreases.[50] Here we find a significantly stronger effect on the morphology. The molten perfluorinated chains can obviously adopt a higher degree of molecular curvature, which leads to smaller perforations. Facets were also observed with stomatosomes, in particular with those formed by amphiphile **6** ([G2]-(C_0-R_f)$_2$) (*cf.* Fig. 7b and d), and they disappeared above 70 °C. The finding of a reduced hole size induced upon chain melting renewed the questions of thermal assembly stability and whether the high temperature state can be frozen. Therefore, we carried out additional annealing experiments.

The morphological changes on the supramolecular level within two hours of annealing in the molten state of perfluorinated chains and subsequent cooling to ambient temperature are demonstrated in Fig. 14. The figure shows image sections from larger cryo-TEM micrographs (Fig. S4 and S5 in the ESI†) of compound **7** ([G2]-(C_3-R_f)$_2$) taken prior and after 2 h of annealing at 60 °C (vitrification after cooling down to ambient temperature), respectively. Before annealing the sample showed prototypical stomatosomes and patches of perforated layers (Fig. 14a). During annealing several stomatosomes lost their high contrast rim or developed an asymmetric density profile (Fig. 14a and b) characterized by a directional gradual fading of the contrast. This structural pattern coincides with one of those already described in the context of Fig. 9a (bottom). The comparison of structures points to a structure rearrangement after long-term equilibration in the state of the molten fluorinated chains. Obviously, the hollow stomatosomes show a tendency to convert into three-dimensional bicontinuous networks comparable to those shown in Fig. 9. The analysis of micrographs also shows many stomatosomes remaining completely unchanged compared to the original state. High temperature structures with significantly smaller perforations could not be obtained. The present amphiphile differs in this regard from a similar capsule-forming amphiphile, which was reported[31] to show a temperature controlled opening of pores.

Generation 3 derivatives. The double-chained analogues with [G3] head groups (**9** ([G3]-(C_3-R_f)$_2$), **10** ([G3]-(C_6-R_f)$_2$)) are readily soluble in water and showed the formation of micelles with ∼5.5 and ∼7 nm diameter (estimated by TEM, whereas the hydrodynamic diameter measured by DLS is again larger), respectively (Fig. S6 in the ESI†). These results are in qualitative

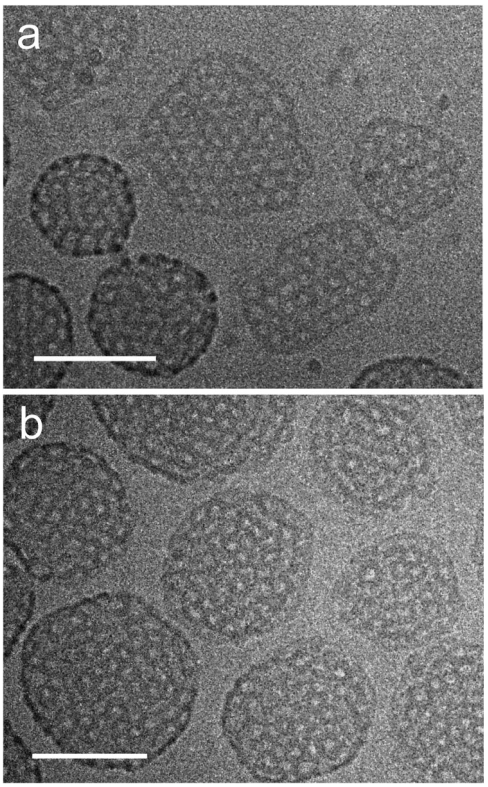

Fig. 14 Cryo-TEM images of compound **7** ([G2]-(C_3-R_f)$_2$) prepared at ambient temperature prior (a) and after (b) annealing for two hours at 60 °C. Concentration: 1% (w/v). Scale bar is 100 nm.

agreement with the corresponding investigations of single-chained [G3] compounds. Despite the presence of a second hydrophobic chain, the bulkier dendritic head group dictates their self-assembly, resulting in small, most probably spherical micelles, *i.e.* aggregates of the highest interfacial curvature.

Mixtures of amphiphiles

We showed before that the size of the dendritic head group determines the molecular asymmetry and hence the morphology of assemblies. Amphiphiles with large [G3] head groups form small micelles throughout, while those with [G1] and [G2] head groups self-assemble into non-spherical, more extended structures, which range from narrow ribbons over perforated bilayers up to bicontinuous three-dimensional networks. From these observations we expected that a finer tuning of molecular asymmetry should be possible by the mixing of the compounds, as has been extensively reported in the literature.[28,51,52]

In two variants we studied mixtures with identical generations of head groups and different hydrophobic tails and *vice versa*. Furthermore, we were interested in the kinetics of structure formation upon mixing both at ambient temperature and upon annealing. Both procedures were expected to eventually reveal identical structures but on different time scales.

In the case of a 1 : 1 (v/v) mixture of amphiphiles **7** and **10** ([G2]-(C_3-R_f)$_2$/[G3]-(C_6-R_f)$_2$) differing in the head group generation (differences in the spacer length can be neglected as outlined before) we followed the morphological changes at ambient temperature over a couple of weeks. 30 minutes after mixing the morphologies known from the pure individual components, *i.e.* stomatosomes (**7** [G2]-(C_3-R_f)$_2$) and spherical micelles (**10** [G3]-(C_6-R_f)$_2$), coexist (not shown). Within three days of storage, nearly all stomatosomes disappeared and became replaced by populations of spherical and worm-like micelles. The spherical micelles became disc-like over the following three weeks (Fig. 15a–c). The findings illustrate a rather slow molecular exchange process under ambient conditions. The process can, however, be accelerated by an annealing process (at 75 °C) performed over only a few hours and eventually yields comparable results.

Equivalent results were obtained for mixtures of amphiphiles with identical [G2] head groups but different numbers of hydrophobic chains. For example we report the results of a 1 : 1 (v/v) mixture of the double tail compound **7** ([G2]-(C_3-R_f)$_2$) and the single chained compound **4** ([G2]-C_{11}-R_f). The latter forms spherical micelles of ~7 nm diameter on its own (not shown). After annealing for 1.5 hours at 75 °C the mixtures morphology is dominated by small micelles, but few worm-like micelles can also be seen (Fig. 16a). A closer inspection reveals that the small micellar aggregates became disc-like. An average diameter of ~8.5 nm and a thicknesses of ~5 nm have been estimated from the top and side view orientations (Fig. 16b and c). The worm-like micelles prove to be narrow ribbons. Their thickness agrees with that of the disc-like micelles. These data are consistent with the obtained for the first ([G2]/[G3]) mixture under ambient conditions after 40 days (Fig. 15c).

Discussion

The supramolecular behavior of the perfluorinated dendritic amphiphiles is principally in good agreement with the well-known concept of the molecular packing parameter.[12] According to this the preferred shape of aggregates is determined by the asymmetry or spontaneous curvature of the amphiphilic molecule, quantified by a specific ratio of $\nu/a_0 l_c$, where ν is the volume of the hydrophobic tail, a_0 is the effective area of the molecule and l_c is the (critical) length of the hydrophobic tail. In dilute amphiphile solutions (~1%) one observes spherical micelles followed by discoidal, cylindrical, and branched micelles, perforated and smooth bilayers upon decreasing the molecular asymmetry.[53] At a higher concentration the assembly structures interact in terms of dense packing towards cubic micellar, hexagonally-packed cylindrical, and lamellar mesophases,[54] wherein bicontinuous three-dimensionally periodic structures have frequently been observed as intermediates between the hexagonal and lamellar phases.[55–57] These trends are reproduced for the most part of the investigated amphiphiles, but also some novel and highly intriguing aspects emerged.

All [G3] derivatives form spherical micelles irrespective of the number of hydrophobic chains. The volume of the head group and hence the molecular asymmetry is so large that it dominates the assembly process in all cases including the double-chained compounds. Also for the single-tailed [G2]

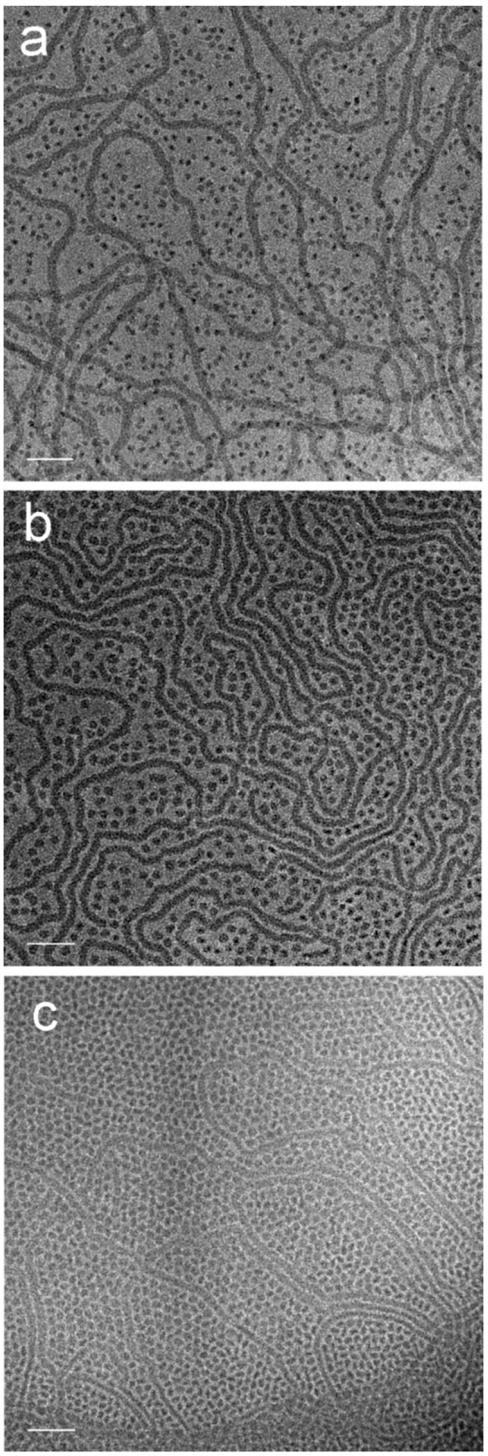

Fig. 15 Cryo-TEM images of a 1 : 1 (v/v) mixture of compounds **7** and **10** ([G2]-(C_3-R_f)$_2$, [G3]-(C_6-R_f)$_2$) taken (a) 3 d, (b) 18 d, and (c) 40 d after mixing at 20 °C. Amphiphile concentration after mixing: 0.5%. Scale bars are 50 nm.

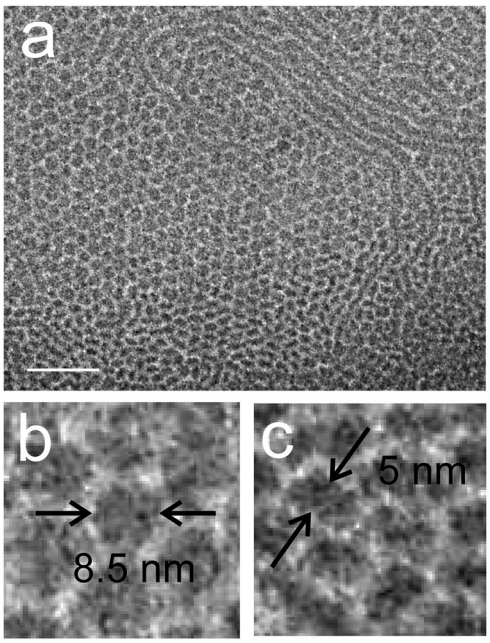

Fig. 16 (a) Cryo-TEM images of a 1 : 1 (v/v) mixture of compounds **7** ([G2]-(C_3-R_f)$_2$) and **4** ([G2]-C_{11}-R_f) after annealing for 1.5 hours at 75 °C. Amphiphile concentration after mixing: 0.5%. Scale bar is 50 nm. (b and c) Magnified sections reveal a disc-like morphology of the small micelles and a ribbon-like structure for the fibrous assemblies.

derivatives the molecular asymmetry is still sufficiently large to favour spherical micelles. The morphology only changes when the head group size continues to decrease as for [G1] derivatives with a single tail. Ribbons instead of cylindrical micelles with spherical cross-section are formed by **1** ([G1]-(C_3-R_f)) and can be ascribed to the specific stiffness of the fluorinated chain segments favoring a flat aggregate morphology.

Surprisingly, the [G1] compound **2** ([G1]-C_6-R_f) with a longer spacer (C_6 *versus* C_3) for compound **1** ([G1]-C_3-R_f) forms highly branched structures (the irregularly perforated vesicles and networks shown in Fig. 3c) instead of the expected linear worm-like micelles. They can be characterized as an intermediary stage in a transition process to the structurally more perfect stomatosomes (see below). The length of the alkyl spacer has obviously a significant effect on the aggregate morphology of compounds **1** and **2**, although the ratio of hydrophobic volume to chain length (*i.e.* the chain cross-section area) is a constant[58] and should not affect the packing parameter and aggregate morphology.[59] This finding indicates an implicit effect of chain length on aggregate structure, which we already observed for fully hydrogenated variants of the present dendritic amphiphiles,[4] and which has recently been rationalized by thermodynamic considerations.[59]

According to the packing concept disk-like micelles should appear between spherical and worm-like micelles.[26,53] They have not been observed for the entire family of amphiphiles investigated here, due to the inadequate spontaneous curvature of molecules. However, they could be generated through the fine tuning of mean spontaneous curvature in binary amphiphile mixtures. Our observation of a limited growth of the disc-like micelles is in agreement with other studies[60] and recent theoretical considerations predicting conditions for their formation.[61] It is, however, not clear if the amphiphiles, which form spherical micelles on its own, are accumulated at

the high curvature edges of the discs,[26,62,63] or if the two amphiphiles mix homogenously over the entire assembly.

Although a reduction of the effective spontaneous curvature by mixing compounds of different molecular asymmetry provides the possibility of a morphological fine-tuning, a marked reduction to a value favoring extended bilayer structures was not observed. Planar bilayer structures are only visible on the local scale for the narrow ribbons and the discoidal aggregates. In this way they have a local precursor in the branching points of the network structures, which is a very typical phenomenon observed with fluorinated amphiphiles.

The most interesting phenomena is the formation of stomatosomes that were observed in a regime of spontaneous curvature approaching a more balanced head-to-tail ratio, such as that present in double-tail [G2] dendritic amphiphiles (Fig. 1). The observation of stomatosomes was so far limited to very restricted experimental conditions and was never found as a stable supramolecular assembly structure for a single-component system. Because the ratio of the tail volume (ν) and the tail length (l_c), is a constant (namely the tail cross-section) the packing parameter and aggregate morphology should not be influenced by the tail length. This is evident for the [G2] compounds **6** ([G2]-(C_0-R_f)$_2$), **7** ([G2]-(C_3-R_f)$_2$), and **8** ([G2]-(C_6-R_f)$_2$) with two tails but differing spacer lengths (C_0 to C_6).

Stomatosomes can be considered as a special kind of vesicle for which the membrane is not continuous but randomly or hexagonally perforated. Particularly in multi-layered stomatosomes also tightly packed layers were found (Fig. 7d), which resemble lamellar structure elements of the hexagonally perforated layer phase (PL) of block copolymers. As the PL phase appeared as an unstable transition structure between the lamellar and gyroid phases[64–66] the aspect of stability arises. Almgren and coworkers[26] have already considered a non-equilibrium nature of stomatosomes. In this respect our annealing experiments suggest such a transition from stomatosomes towards three-dimensional bicontinuous network structures (Fig. 9 and 10) indicating a further step towards a final equilibrium structure.

While the interfacial curvature of aggregates set by the spontaneous curvature of molecules, optimizes the enthalpy of the micellar system, end caps and branch junction points increase the entropy by increasing the number of micelles or the number of possible configurations. Thus, these topological defects stabilize the micellar population. As has been discussed by Safran *et al.*,[28] the type of defect, which dominates the morphological behavior, depends to a certain degree on the amphiphiles' spontaneous curvature. Accordingly, amphiphiles with low spontaneous curvature should favor branching and network structures. This seems to be the case here. The stiffness of frozen fluorinated chains favors a lower spontaneous curvature and can thus rationalize the predominance of branched micellar structures. We observed that heating to the molten state only led to smaller perforations in the stomatosomes (high temperature experiment, Fig. 14), *i.e.* increased mean interfacial curvature, but not to a marked reduction in the degree of branching. Long-term annealing above the melting temperature and subsequent cooling had no lasting effect on the structure, *i.e.* the size of the perforations.

The 3D mesh structures required a more detailed investigation as we noticed differences in the structural organization, which were not obvious at first sight, in particular by inspection of two-dimensional projection images alone. Cryo-ET revealed that the perforated layers as well as the stomatosomes can significantly differ in their spatial organization.

The analysis of tomographic data of the networks revealed a structural organization resembling the nanostructure of bicontinuous intermediate phases (Fig. 9 and 10), which were detected for several aqueous amphiphile systems at higher concentrations or for block copolymers.[22,24,67–71] These structures can be mathematically best described by the concept of minimal surfaces.[42] Three essential types of bicontinuous morphologies have been identified, namely an ordered bicontinuous double diamond structure (D), a gyroid structure (G) as well as a cubic structure (P), which are topologically related. Since the discovery of intermediate phases for block copolymers there was a long-lasting debate about the thermodynamic stability of these structures. In the simplest case of diblock copolymers D and G morphologies as well as a randomly or hexagonally perforated layer structure (PL) were theoretically predicted and experimentally observed.[57] Today it is believed to be proven that the PL morphology is a long-lived non-equilibrium state, which converts towards the bicontinuous G phase.[64–66] This highly interesting result casts new light on the thermodynamic stability of complex stomatosome structures.

In contrast to extended structures of intermediate liquid crystalline phases the present meshes exist already at a very low concentration (around 1%), *i.e.* their spatial extension is restricted and they are dispersed in the continuous water phase. Because the concentration dependence has not been investigated in detail it remains unclear if they belong to a one-phase region normally termed L_1 or to another liquid phase (for example the lamellar phase L_α). One could speculate that the mesh fragments represent precursor structures of a respective intermediate phase. In particular, the bicontinuous structures shown in Fig. 9 and 10 show the best correlation with a bicontinuous cubic phase of double diamond symmetry. This behavior is related to reports on the aggregation behavior of Gemini amphiphiles,[45,69] which also tend to form bicontinuous cubic phases at moderate concentration (however, in this case a double gyroid phase). Such a network formation is obviously favored by double chain compounds.

Conclusions

We here interpret the supramolecular morphologies of novel fluorinated non-ionic dendritic amphiphiles within the framework of the well-known concept of molecular packing parameter, which states that the geometry of self-assembled structures is determined by the spontaneous curvature of the molecule.

In contrast to alkyl-tail amphiphiles, the fluorinated tail segments introduce additional chain stiffness thus favoring locally planar architectures. In addition, the bulky dendritic head-groups prefer highly curved assemblies. The combination of these two structural elements leads to the formation of branched and perforated unique architectures. In fact, in the absence of fluorinated tail segments, *i.e.* for the related dendritic amphiphiles with pure alkyl tails as investigated in our former studies,[3–5] branched micelles or perforated vesicles have never been observed.

The new and most important finding is, that with the designed fluorinated dendritic amphiphiles a series of robust non-equilibrium morphologies can be generated spontaneously and reproducibly by simple dissolution of single-component systems in water. So far stomatosomes have only been identified in narrow temperature and concentration limits of multicomponent surfactant and block copolymer systems. In most such systems stomatosomes appear as intermediate structures in a transition process between extended bilayers and cylindrical micelles. Here, we demonstrate for the first time that stomatosomes are metastable and transform into a bicontinuous cubic phase facilitated by a longer annealing process. Another novel aspect is that this phase was observed even in the dilute concentration regime of only 1 wt%. By solely adopting the appropriate molecular structure robust entities can be generated by a single-component system.

Conflicts of interest

There are no conflicts of interest to declare.

Acknowledgements

We would like to thank the Focus Area Nanoscale of the Freie Universität Berlin for financial support and the assistance of the Core Facility BioSupraMol. We thank K. Biskup and P. Hommes for help with synthesis and W. Münch for his help with HPLC purification.

References

1 D. Tomalia, J. Christensen and U. Boas, *Dendrimers, Dendrons and Dendritic Polymers, Discovery, Applications, and the Future*, Cambridge University Press, Cambridge, 2012.
2 A. Mohr and R. Haag, in *Applications of Supamolecular Chemistry*, ed. H.-J. Schneider, CRC Press, Tayler & Francis, Boca Raton, 2012, p. 341.
3 B. Trappmann, K. Ludwig, M. R. Radowski, A. Shukla, A. Mohr, H. Rehage, C. Böttcher and R. Haag, *J. Am. Chem. Soc.*, 2010, **132**, 11119–11124.
4 B. N. S. Thota, H. v. Berlepsch, C. Böttcher and R. Haag, *Chem. Commun.*, 2015, **51**, 8648–8651.
5 S. Kumar, K. Ludwig, B. Schade, H. V. Berlepsch, I. Papp, R. Tyagi, M. Gulia, R. Haag and C. Böttcher, *Chem. – Eur. J.*, 2016, **22**, 5629–5636.
6 P. Degen, M. Wyszogrodzka and C. Strötges, *Langmuir*, 2012, **28**, 12438–12442.
7 C. M. Jäger, A. Hirsch, C. Böttcher and T. Clark, Proceedings of the Beilstein Symposium, ''Functional Nanoscience'', 2011, pp. 91–106.
8 M. S. Becherer, B. Schade, C. Böttcher and A. Hirsch, *Chem. – Eur. J.*, 2009, **15**, 1637–1648.
9 M. Kellermann, W. Bauer, A. Hirsch, B. Schade, K. Ludwig and C. Böttcher, *Angew. Chem., Int. Ed.*, 2004, **43**, 2959–2962.
10 (*a*) J.-N. Marsat, M. Heydenreich, E. Kleinpeter, H. V. Berlepsch, C. Böttcher and A. Laschewsky, *Macromolecules*, 2011, **44**, 2092–2105; (*b*) H. V. Berlepsch, C. Böttcher, K. Skrabania and A. Laschewsky, *Chem. Commun.*, 2009, 2290–2292.
11 Z. Li, E. Kesselmann, Y. Talmon, M. A. Hillmyer and T. P. Lodge, *Science*, 2004, **306**, 98–101.
12 J. N. Israelachvili, D. J. Mitchel and B. W. Ninham, *J. Chem. Soc., Faraday Trans.*, 1976, **172**, 1525–1568.
13 A. Garcia-Bernab, C. C. Tzschucke, W. Bannwarth and R. Haag, *Adv. Synth. Catal.*, 2005, **347**, 1389–1394.
14 M. Zieringer, A. Garcia-Bernab, B. Costisella, H. Glatz, W. Bannwarth and R. Haag, *ChemPhysChem*, 2010, **11**, 2617–2622.
15 P. D. I. Fletcher, *Specialist Surfactants*, ed. I. D. Robb, Chapman & Hall, 1997, ch. 5, pp. 104–142.
16 M. Monduzzi, *Curr. Opin. Colloid Interface Sci.*, 1998, **3**, 467–477.
17 K. Matsuoka and Y. Moroi, *Curr. Opin. Colloid Interface Sci.*, 2003, **8**, 227–235.
18 E. Kissa, *Fluorinated Surfactants and Repellents*, Surfactant science series, Marcel Dekker, Inc., NY, 2nd edn, 2001, ch. 3, vol. 97, p. 80.
19 T. Kunitake and N. Higashi, *J. Am. Chem. Soc.*, 1985, **107**, 692–696.
20 J. G. Riess, *J. Drug Targeting*, 1994, **2**, 455–468.
21 E. Buhler, C. Oelschlaeger, G. Waton, M. Rawiso, J. Schmidt, Y. Talmon and S. J. Candau, *Langmuir*, 2006, **22**, 2534–2542.
22 P. Kekicheff and G. J. T. Tiddy, *J. Phys. Chem.*, 1989, **93**, 2520–2526.
23 M. C. Holmes, M. S. Leaver and A. M. Smith, *Langmuir*, 1995, **11**, 356–365.
24 S. Puntambekar, M. C. Holmes and M. S. Leaver, *Liq. Cryst.*, 2000, **27**, 743–747.
25 R. Oda, I. Huc, D. Danino and Y. Talmon, *Langmuir*, 2000, **16**, 9759–9769.
26 M. Almgren, *Soft Matter*, 2010, **6**, 1383–1390.
27 R. Zhou, M. Leaver, R. McCabe and M. Holmes, *Soft Matter*, 2012, **8**, 12255–12261.
28 N. Dan and S. A. Safran, *Adv. Colloid Interface Sci.*, 2006, **123-126**, 323–331.
29 M. Tang and W. C. Carter, *J. Phys. Chem. B*, 2013, **117**, 2898–2905.
30 C. Breyton, F. Gabel, M. Abla, Y. Pierre, F. Lebaupain, G. Durand, J.-L. Popet, C. Ebel and B. Pucci, *Biophys. J.*, 2009, **97**, 1077–1086.
31 J.-K. Kim, E. Lee, Y.-B. Lim and M. Lee, *Angew. Chem., Int. Ed.*, 2008, **47**, 4662–4666.

32 H. Oh, A. M. Ketner, R. Heymann, E. Kesselman, D. Danino, D. E. Falvey and S. R. Raghabvan, *Soft Matter*, 2013, **9**, 5025–5033.
33 L. M. Bergström, S. Skoglund, K. Edwards, J. Eriksson and I. Grillo, *Langmuir*, 2014, **30**, 3928–3938.
34 C. K. Haluska, W. T. Góźdź, H.-G. Döbereiner, S. Förster and G. Gompper, *Phys. Rev. Lett.*, 2002, **89**, 238302.
35 W. Zhao, D. Chen, Y. Hu, G. M. Grason and T. P. Russell, *ACS Nano*, 2011, **5**, 486–492.
36 D. J. A. Crommelin and H. Schreier, Liposomes, in *Colloidal Drug Delivery Systems*, ed. J. Kreuter, Marcel Dekker Inc., New York, 1994, ch. 3, p. 73.
37 M. Rappolt, in *Advances in Planar Lipid Bilayers and Liposomes*, ed. A. Leitmannova Liu, Elsevier, USA, 2007, ch. 9, vol. 5, p. 254.
38 V. Lucic, F. Forster and W. Baumeister, *Annu. Rev. Biochem.*, 2005, **74**, 833–865.
39 A. L. Parry, P. H. Bomans, S. J. Holder, N. A. Sommerdijk and S. C. Biagini, *Angew. Chem., Int. Ed.*, 2008, **47**, 8859–8862.
40 T. I. Löbling, J. S. Haataja, C. V. Synatschke, F. H. Schacher, M. Müller, A. Hanisch, A. H. Gröschel and A. H. E. Müller, *ACS Nano*, 2014, **8**, 11330–11340.
41 Amira Software Version 6.0.0, Thermo Fisher Scientific, Hillsboro, Oregon, USA.
42 A. D. Benedicto and D. F. O'Brien, *Macromolecules*, 1997, **30**, 3395–3402.
43 W. Longley and T. J. McIntosh, *Nature*, 1983, **303**, 612–614.
44 P. Mariani, V. Luzzati and H. Delacroix, *J. Mol. Biol.*, 1988, **204**, 165–189.
45 D. V. Perroni, C. M. Baez-Cotto, G. P. Sorenson and M. K. Mahanthappa, *J. Phys. Chem. Lett.*, 2015, **6**, 993–998.
46 C. Y. Chu, X. Jiang, H. Jinnai, R. Y. Pei, W. F. Lin, J. C. Tsai and H. L. Chen, *Soft Matter*, 2015, **11**, 1871–1876.
47 Y.-C. Wang, M. Wakabayashi, H. Hasegawa and M. Takenaka, *Soft Matter*, 2017, **13**, 8824–8828.
48 M. P. N. Gent and C. Ho, *Biochemistry*, 1978, **17**, 3023–3038.
49 P. M. Frederik, M. C. A. Stuart, P. H. H. Bomans, W. M. Busing, K. N. J. Burger and A. J. Verkleij, *J. Microsc.*, 1991, **161**, 253–262.
50 J. F. Nagle, *Annu. Rev. Phys. Chem.*, 1980, **31**, 157–195.
51 S. A. Safran, P. Pincus and A. Andelman, *Science*, 1990, **248**, 354–356.
52 S. Jain and F. S. Bates, *Macromolecules*, 2004, **37**, 1511–1523.
53 G. Porte, R. Gomati, O. El Haitamy, J. Appell and J. Marignan, *J. Phys. Chem.*, 1986, **90**, 5746–5751.
54 D. J. Mitchell, G. J. T. Tiddy, L. Waring, T. Bostock and M. P. McDonald, *J. Chem. Soc., Faraday Trans. 1*, 1983, **79**, 975–1000.
55 M. C. Holmes, *Curr. Opin. Colloid Interface Sci.*, 1998, **3**, 485–492.
56 C. Tschierske, *Curr. Opin. Colloid Interface Sci.*, 2002, **7**, 69–80.
57 M. W. Matsen and F. S. Bates, *Macromolecules*, 1996, **29**, 7641–7644.
58 C. Tanford, *The Hydrophobic Effect*, Wiley-Interscience, New York, 1973.
59 R. Nagarajan, *Langmuir*, 2002, **18**, 31–38.
60 L. van Dam, G. Karlsson and K. Edwards, *Biochim. Biophys. Acta*, 2004, **1664**, 241–256.
61 P. A. Kralchevsky, K. D. Danov, S. E. Anackov, G. S. Georgieva and K. P. Ananthapadmanabhan, *Curr. Opin. Colloid Interface Sci.*, 2013, **18**, 524–531.
62 R. R. Vold and R. S. Prosser, *J. Magn. Reson., Ser. B*, 1996, **113**, 267–271.
63 M. J. Greenall, *Macromolecules*, 2016, **49**, 723–730.
64 D. A. Hajduk, H. Takenouchi, M. A. Hillmyer and F. S. Bates, *Macromolecules*, 1997, **30**, 3788–3795.
65 I. W. Hamley, V. Castelletto, O. O. Mykhaylyk, Z. Yang, R. P. May, K. S. Lyakhova, G. J. A. Sevink and A. V. Zvelindovsky, *Langmuir*, 2004, **20**, 10785–10790.
66 N. Ji, P. Tang and F. Qiu, *Macromolecules*, 2015, **48**, 8681–8693.
67 C. E. Fairhurst, M. C. Holmes and M. S. Leaver, *Langmuir*, 1997, **13**, 4964–4975.
68 C. K. Liu and G. G. Warr, *Langmuir*, 2015, **31**, 2936–29454.
69 G. P. Sorenson, A. K. Schmitt and M. K. Mahanthappa, *Soft Matter*, 2014, **10**, 8229–8235.
70 S. Mazzoni, L. R. S. Barbosa, S. S. Funari, R. Itri and P. Mariani, *Langmuir*, 2016, **32**, 873–881.
71 Y. Chen, J. Du, M. Xiong, H. Guo, H. Jinnai and T. Kaneko, *Macromolecules*, 2007, **40**, 4389–4392.